

Three-level atom interferometer with bichromatic laser fields

Kazuhiro Honda, Shinya Yanagimachi,* and Atsuo Morinaga

Faculty of Science and Technology, Tokyo University of Science, 2641 Yamazaki, Noda-shi, Chiba 278-8510, Japan

(Received 6 June 2003; published 20 October 2003)

We have developed a three-level atom interferometer using three-level atoms coupled with bichromatic fields in order to investigate the phase information between two excited states. First, we presented a theoretical description of the interaction of three-level atoms with bichromatic fields based on single-transition operators. Using the time evolution of a wave function, the equations of the interference fringes and the visibility were derived and calculated for several types of the three-level atom interferometers with bichromatic fields. Optimum excitation conditions were evaluated. Next, several types of three-level atom interferometers were demonstrated experimentally using a thermal calcium atomic beam with two Zeeman substates of $m=1$ and $m=-1$ in the long-lived excited state coupled with bichromatic resonant fields between the ground state and the excited states. The behaviors of the interference fringes were compared among them along with the calculated results. The three-level atom interferometer excited by two bichromatic laser beams separated in space was found to produce the largest visibility among them when the excitation power of each frequency component was the same.

DOI: 10.1103/PhysRevA.68.043621

PACS number(s): 03.75.Dg, 07.60.Ly, 32.80.Lg, 42.50.Vk

I. INTRODUCTION

During the past ten years, Ramsey-Bordé atom interferometers have been developed as indispensable tools of frequency standards [1], sensitive detection for precise measurements [2,3], and fundamental tests of quantum physics [4]. Most of these experiments were achieved by the conventional Ramsey-Bordé atom interferometers composed of a two-level atom. The atom interferometer consists of the ground state and a long-lived excited state coupled with a resonant laser beam between them [5]. The two wave packets of the ground state and the excited state are split and are recombined by use of the interaction with a resonant light. Then the phase difference between two wave packets caused by a perturbation before recombination is observed as the phase of interference fringes appeared in the population probability of the ground state or the excited state. The phase in the ground state differs by π rad from that in the excited state. The amplitude or visibility of the interference fringes can be calculated using the evolution of spinor operators derived by Bordé *et al.* [6].

Such a two-level atom interferometer (hereafter, atom interferometer is referred to as AI) works like a polarizing interferometer in optics, so that the difference of the electromagnetic properties between the two states could be investigated under an electromagnetic field. In particular, the symmetrical Ramsey-Bordé AI demonstrated by Morinaga and Ohuchi [7] is useful because the phase is free from the fluctuation of the laser frequency. For instance, the phase shift between the 3P state and 1S state of calcium atoms due to the Stark effect was clearly observed [8]. However, there is a case where it is desirable to investigate the phase difference between two long-lived excited states. Then, the three-level

AI which is composed of two excited states and a ground state will be required.

Up to now, several types of three-level AIs were developed. Chu *et al.* developed the three-level AI using stimulated two-photon Raman transitions between the ground hyperfine states of sodium atoms and an intermediate excited state [9]. The amplitude of the interference fringes was analyzed by his group in detail [10]. Consequently, it was found that this three-level system reduced to a two-level system by adiabatic elimination of the intermediate state. Ertmer and co-workers [11] developed a three-level AI with two excited states, which are coupled with a monochromatic laser beam simultaneously. The interference signal was calculated using the concept of momentum families of the two-level AI as described by Bordé *et al.* [6]. Furthermore, a multilevel interferometer was developed by Hänsch and co-workers [12], but it is not related specifically to the Ramsey-Bordé AI.

On the other hand, we have developed three-level AIs using calcium atoms in order to observe the Aharonov-Casher phase difference between the Zeeman sublevels $m=1$ and $m=-1$. First, we developed a three-level AI, which was excited by two parallel laser beams with one resonant frequency and by another equally spaced two parallel laser beams with the other resonant frequency [13]. Next, we have developed a three-level AI excited by two bichromatic fields [14]. The AI was composed of the ground 1S_0 state and two nondegenerated Zeeman sublevels of $m=1$ and $m=-1$ in the 3P_1 state which were coupled with σ^+ and σ^- polarized beams, respectively. The atom was excited by bichromatic σ^+ and σ^- laser beams, simultaneously, at two points separated spatially. The phase difference between the two Zeeman sublevels was analyzed and it was found that both phases of interference of the Zeeman sublevels are the same after the recombination, so that the interference fringes are enhanced. Consequently, the interference signal could be observed in the sum of the fluorescence signal from both excited states. Conversely, the fringe phase of the excited states differs by π rad from that of the ground state. It should be

*Present address: National Metrology Institute of Japan, AIST Tsukuba central 3, 1-1, Umezono, Tsukuba-shi, Ibaraki 305-8563, Japan.

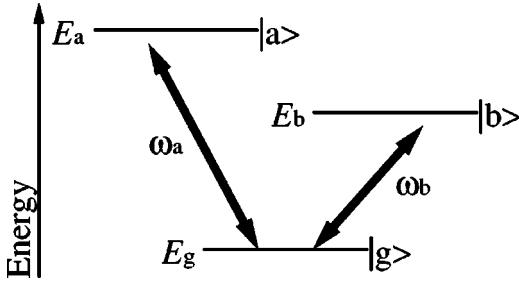


FIG. 1. Energy diagram of the three-level atom and bichromatic field. The frequencies ω_a and ω_b of the bichromatic field are tuned to the resonance frequencies of transitions $|g\rangle\text{-}|a\rangle$ and $|g\rangle\text{-}|b\rangle$, respectively.

noted that this three-level AI differs from the AI using the stimulated Raman transitions at this point. Thus, various kinds of three-level AIs using the three-level atom and the bichromatic laser fields are possible to produce. Therefore, the three-level AI will become a powerful tool as a polarizing AI. However, the amplitude and visibility of the interference fringes of the three-level system cannot be calculated using the evolution of spinor operators, which was used in the two-level system [6]. To the best of our knowledge, there has been no report presenting formulas for the three-level AI with bichromatic fields.

In the present paper, we discuss the interference fringes of the three-level AIs theoretically and experimentally. In Secs. II and III, we derive a theoretical framework and description for the interference fringes of the three-level AI excited with bichromatic laser fields in terms of single-transition operators [15] and we present the calculated results of the interference fringes and visibilities for the three-level AIs of several excitation schemes. In Sec. IV, we demonstrate a different scheme of the three-level AI experimentally and compare the visibilities among the three schemes of the three-level AI along with the calculated results.

II. INTERACTION OF A THREE-LEVEL ATOM AND BICHROMATIC FIELD

We consider a three-level atom which is composed of a ground state $|g\rangle$ and two long-lived excited states $|a\rangle$ and $|b\rangle$, as shown in Fig. 1. The energies of states $|g\rangle$, $|a\rangle$, and $|b\rangle$ are E_g , E_a , and E_b , respectively. It is assumed that the atom moves with a velocity of $\mathbf{v}=(v_x, v_y, v_z)$ and a laser beam propagates parallel to the z axis. The laser beam is a bichromatic field whose frequencies are ω_a and ω_b , which are tuned to the resonance frequencies of transitions $|g\rangle\text{-}|a\rangle$ and $|g\rangle\text{-}|b\rangle$, respectively. The electric field of the laser beam can be written in the classical description as

$$\mathbf{E}(\mathbf{r}, t) = \sum_{n=a,b} \boldsymbol{\epsilon}_n A_n \cos(\gamma \omega_n t - k_n z - k_n v_z t + \phi_n), \quad (1)$$

where k_n is the wave number, $\boldsymbol{\epsilon}_n$ is the polarization vector, A_n and ϕ_n are the amplitude and the phase of each frequency component of the field, and $\gamma = \sqrt{1 - v^2/c^2}$ is the relativity effect which causes a higher-order Doppler effect. We assume that the field of frequency ω_a only couples states $|g\rangle$

and $|a\rangle$, while the field of ω_b only couples states $|g\rangle$ and $|b\rangle$. This assumption can be true strictly for photon polarization or for an energy split between states $|a\rangle$ and $|b\rangle$, which is larger than the resonance widths of the transitions.

When the interaction of the atom and the field is assumed to be the electric dipole interaction, the Hamiltonian can be written in the semiclassical description as

$$\hat{H} = \frac{p^2}{2m} + \sum_{l=g,a,b} \left(E_l - i \frac{\hbar \Gamma_l}{2} \right) |l\rangle\langle l| - \sum_{n=a,b} \mathbf{d}_n \cdot \mathbf{E}, \quad (2)$$

where m and \mathbf{p} are the mass and the momentum of the atom and Γ_l is the relaxation rate of the $|l\rangle$ state. The electric dipole moment of the transition $|g\rangle\text{-}|n\rangle$ is \mathbf{d}_n and $\mathbf{d}_a \cdot \mathbf{E}_b = \mathbf{d}_b \cdot \mathbf{E}_a = 0$ is assumed from the resonant condition.

This Hamiltonian is rewritten by using the ‘‘single-transition operators’’ $S_{x,y,z}^{rs}$ [15,16], which facilitate the transfer of the results from the analysis of the two-level system to the three-level system. The single-transition operators are defined as

$$\begin{aligned} \langle r | S_x^{rs} | s \rangle &= (\tfrac{1}{2}), & \langle s | S_x^{rs} | r \rangle &= \tfrac{1}{2}, \\ \langle r | S_y^{rs} | s \rangle &= (-i/2), & \langle s | S_y^{rs} | r \rangle &= i/2, \\ \langle r | S_z^{rs} | r \rangle &= (\tfrac{1}{2}), & \langle s | S_z^{rs} | s \rangle &= -\tfrac{1}{2}, \end{aligned} \quad (3)$$

and zero otherwise, where r and s are g , a , and b . These include ‘‘spin operators’’ for the two-level atom in the components involved with the $|r\rangle$ and $|s\rangle$ states. In addition, we define the level-shift operators $\Sigma_{g,a,b}$ in the 3×3 matrix form as

$$\begin{aligned} \Sigma_g &= \begin{pmatrix} 0 & 0 & 0 \\ 0 & 0 & 0 \\ 0 & 0 & 1 \end{pmatrix}, & \Sigma_a &= \begin{pmatrix} 0 & 0 & 0 \\ 0 & 1 & 0 \\ 0 & 0 & 0 \end{pmatrix}, \\ \Sigma_b &= \begin{pmatrix} 1 & 0 & 0 \\ 0 & 0 & 0 \\ 0 & 0 & 0 \end{pmatrix}. \end{aligned} \quad (4)$$

Here, the wave-function vector of the atom is ${}^t(c_b, c_a, c_g)$ with a probability amplitude c_i of the $|i\rangle$ state.

When the initial atom momentum is perpendicular to the propagation direction of the laser beam, the Hamiltonian is

$$\begin{aligned} \frac{\hat{H}}{\hbar} &= - \left(\frac{iE_g}{\hbar} + \frac{\Gamma_g}{2} \right) \Sigma_g - \left(\frac{iE_a}{\hbar} + i\delta_a + \frac{\Gamma_a}{2} \right) \Sigma_a \\ &\quad - \left(\frac{iE_b}{\hbar} + i\delta_b + \frac{\Gamma_b}{2} \right) \Sigma_b \\ &\quad + 2i\Omega_a \cos(\gamma \omega_a t - k_a v_z t - k_a z + \phi_a) S_x^{ga} \\ &\quad + 2i\Omega_b \cos(\gamma \omega_b t - k_b v_z t - k_b z + \phi_b) S_x^{bg}, \end{aligned} \quad (5)$$

where $\delta_n = \hbar \mathbf{k}_n^2 / 2m$ is the recoil shift and $\Omega_n = |\mathbf{d}_n \cdot \boldsymbol{\epsilon}_n A_n| / \hbar$ is the Rabi frequency. In this equation, the initial kinetic energy of the atom is excluded.

In order to eliminate the time-dependent terms in the Hamiltonian, the rotating-wave approximation is applied to the transitions $|g\rangle\text{-}|a\rangle$ and $|g\rangle\text{-}|b\rangle$ [15]. The Hamiltonian in the rotating frame \hat{H}_R becomes

$$\begin{aligned} \frac{\hat{H}_R}{i\hbar} \approx & i\Delta_a \Sigma_a + i\Delta_b \Sigma_b + i\Omega_a (\cos\phi_a S_x^{ga} - \sin\phi_a S_y^{ga}) \\ & + i\Omega_b (\cos\phi_b S_x^{bg} + \sin\phi_b S_y^{bg}), \end{aligned} \quad (6)$$

where

$$\Delta_n = \gamma\omega_n - \frac{E_n - E_g}{\hbar} - \delta_n + i\frac{\Gamma_n - \Gamma_g}{2} - k_n v_z. \quad (7)$$

The evolution of the atomic wave function $\psi_R(t)$ in the rotating frame is given by the Schrödinger equation

$$i\hbar \frac{d\psi_R(t)}{dt} = \hat{H}_R \psi_R(t). \quad (8)$$

When $\psi_R(t)$ is denoted as $\psi_R(t) = {}^t(c_b c_a c_g)$, the Hamiltonian can be deduced in the 3×3 matrix form as follows:

$$\frac{d\psi_R(t)}{dt} = \begin{pmatrix} i\Delta_b & 0 & i\frac{\Omega_b}{2} e^{-i\phi_b} \\ 0 & i\Delta_a & i\frac{\Omega_a}{2} e^{-i\phi_a} \\ i\frac{\Omega_b}{2} e^{i\phi_b} & i\frac{\Omega_a}{2} e^{i\phi_a} & 0 \end{pmatrix} \psi_R(t). \quad (9)$$

Generally, the equation must be resolved numerically, but it can easily be solved analytically in the following case.

A. Case I: Field-free zone

In the field-free zone, each state of the atom evolves independent of each other, so that the time evolution of the wave function can be obtained as

$$\psi_R(t) = [\Sigma_g + e^{i\Delta_a(t-t_0)}\Sigma_a + e^{i\Delta_b(t-t_0)}\Sigma_b] \psi_R(t_0). \quad (10)$$

B. Case II: Monochromatic field

The monochromatic field corresponds to the case where Ω_a or Ω_b is zero. Here, assuming $\Omega_b = 0$, the light field only

couple to the transition $|g\rangle\text{-}|a\rangle$. Then the states $|g\rangle$ and $|a\rangle$ evolve as a two-level system, while state $|b\rangle$ evolves independently. The wave function can be easily solved as

$$\begin{aligned} \psi_R(t) = & \exp\left\{i\frac{\Delta_a}{2}(t-t_0)\right\} \left[\cos\left\{\frac{\Omega'_a}{2}(t-t_0)\right\} (\Sigma_g + \Sigma_a) \right. \\ & + 2i \sin\left\{\frac{\Omega'_a}{2}(t-t_0)\right\} \left\{ -\frac{\Delta_a}{\Omega'_a} S_z^{ga} \right. \\ & \left. \left. + \frac{\Omega_a}{\Omega'_a} (\cos\phi_a S_x^{ga} + \sin\phi_a S_y^{ga}) \right\} \right] \\ & + \exp\left\{i\left(\Delta_b - \frac{\Delta_a}{2}\right)(t-t_0)\right\} \Sigma_b \psi_R(t_0), \end{aligned} \quad (11)$$

where

$$\Omega'_a = \sqrt{\Omega_a^2 + \Delta_a^2}. \quad (12)$$

C. Case III: Bichromatic field

In general, it is difficult to solve the wave function analytically when frequency components of a bichromatic field are resonant with two transition frequencies of the atom. However, it can be resolved easily in the following two cases.

1. $\Delta_a = \Delta_b = \Delta$

This is the case where the detuning of the laser frequency ω_a from the resonance frequency of transition $|b\rangle\text{-}|a\rangle$ is equal to that of ω_b from the resonance frequency of transition $|g\rangle\text{-}|b\rangle$. With the generalized Rabi frequency $\Omega'^2 = \Omega_a^2 + \Omega_b^2 + \Delta^2$, the Hamiltonian is

$$\begin{aligned} \frac{\hat{H}_R}{i\hbar} = & i\Delta(\Sigma_a + \Sigma_b) + i\Omega_a \{\cos\phi_a S_x^{ga} - \sin\phi_a S_y^{ga}\} \\ & + i\Omega_b \{\cos\phi_b S_x^{bg} + \sin\phi_b S_y^{bg}\}. \end{aligned} \quad (13)$$

In the rotating frame, the two excited states are degenerated since their energies are equal. Therefore, two excited states can be mixed and the Hamiltonian can be transformed into the form where one mixed excited state and a ground state $|g\rangle$ evolve like a two-level atom and the other mixed excited state evolves independently. As a result, the time evolution of the wave function is

$$\begin{aligned} \psi_R(t) = & \exp\left\{-i\frac{\Delta}{2}(t-t_0)\right\} \left[\cos\left\{\frac{\Omega'}{2}(t-t_0)\right\} I + \frac{2i}{\Omega'} \sin\left\{\frac{\Omega'}{2}(t-t_0)\right\} \left\{ \Omega_a (\cos\phi_a S_x^{ga} - \sin\phi_a S_y^{ga}) \right. \right. \\ & \left. \left. + \Omega_b (\cos\phi_b S_x^{bg} + \sin\phi_b S_y^{bg}) + \frac{\Omega_a \Omega_b \Delta}{\Omega_e^2} (\cos(\phi_a - \phi_b) S_x^{ab} + \sin(\phi_a - \phi_b) S_y^{ab}) - \Delta S_z^{ga} - \frac{\Omega_b^2 \Delta}{\Omega_e^2} S_z^{ab} \right\} \right. \\ & \left. \times \left(\frac{\Sigma_a + \Sigma_b}{2} - \frac{\Omega_a^2 - \Omega_b^2}{\Omega_e^2} S_z^{ab} - \frac{2\Omega_a \Omega_b}{\Omega_e^2} \{\cos(\phi_a - \phi_b) S_x^{ab} + \sin(\phi_a - \phi_b) S_y^{ab}\} \right) \right] \psi_R(t_0), \end{aligned} \quad (14)$$

with $\Omega_e^2 = \Omega_a^2 + \Omega_b^2$ and I is the identity operator, $\langle n|I|m\rangle = \delta_{nm}$.

2. $\Delta_a = -\Delta_b = \Delta$ and $\Omega_a = \Omega_b = \Omega$

When the magnitudes of two detunings are the same, but their signs are opposite, and the field amplitudes of two frequency components are the same, the evolution of the wave function is

$$\begin{aligned} \psi_R(t) = & \left[\left\{ \frac{4\Delta^2}{\Omega'^2} + \frac{2\Omega^2}{\Omega'^2} \cos \frac{\Omega'}{2} (t-t_0) \right\} \Sigma_g + \left\{ \frac{\Omega^2}{\Omega'^2} + \frac{\Omega^2 + 4\Delta^2}{\Omega'^2} \cos \frac{\Omega'}{2} (t-t_0) \right\} (\Sigma_a + \Sigma_b) + 4i \frac{\Delta}{\Omega'} \sin \frac{\Omega'}{2} (t-t_0) S_z^{ab} \right. \\ & + \frac{2\Omega^2}{\Omega'^2} \left\{ \cos \frac{\Omega'}{2} (t-t_0) - 1 \right\} \left\{ \cos(\phi_a - \phi_b) S_x^{ab} + \sin(\phi_a - \phi_b) S_y^{ab} \right\} + \frac{2\Omega}{\Omega'} \left[\frac{2\Delta}{\Omega'} \left\{ \cos \frac{\Omega'}{2} (t-t_0) - 1 \right\} + i \sin \frac{\Omega'}{2} (t-t_0) \right] \\ & \left. \times (\cos \phi_a S_x^{ga} - \sin \phi_a S_y^{ga}) + \frac{2\Omega}{\Omega'} \left[\frac{2\Delta}{\Omega'} \left\{ 1 - \cos \frac{\Omega'}{2} (t-t_0) \right\} + i \sin \frac{\Omega'}{2} (t-t_0) \right] (\cos \phi_b S_x^{bg} + \sin \phi_b S_y^{bg}) \right] \psi_R(t_0), \quad (15) \end{aligned}$$

with $\Omega'^2 = 4\Delta^2 + 2\Omega^2$.

Of course, the wave functions in the cases III 1 and III 2 are consistent with each other when $\Delta = 0$ and $\Omega_a = \Omega_b$.

III. THREE-LEVEL ATOM INTERFEROMETERS

Atom interferometers are constructed using coherent interactions of an atom with light as a beam splitter. A typical symmetric two-level AI is composed of four copropagating traveling monochromatic laser beams, whose beam spacing of the first two beams is equal to that of the last two beams. Then this AI is comprised of two Mach-Zehnder-type interferometers formed by two pairs of atomic trajectories [17]. The two interferometers differ on the point that the two wave packets of the atom are the ground state or the excited state in the interval between the second and the third beams (center zone). On the other hand, several types of AIs can be constructed by combinations of the three-level atom and

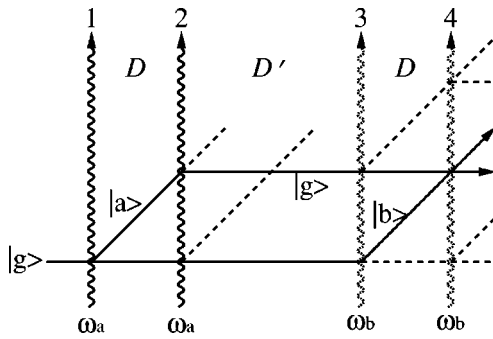


FIG. 2. AI interacting with a sequence of $\omega_a - \omega_a - \omega_b - \omega_b$. Atom trajectories are indicated by straight lines and dashed lines. The atom in the ground state $|g\rangle$ which comes from the left interacts with four copropagating laser beams, indicated by wavy lines. The frequency ω_a of the first and second laser beams is resonant to the transition $|g\rangle - |a\rangle$. The frequency ω_b of the third and fourth laser beams is resonant to the transition $|g\rangle - |b\rangle$. The spacing between the first and the second laser beams is the same as that between the third and the fourth laser beams. The two trajectories indicated by straight lines make a closed loop and the interference signal is generated after the fourth interaction.

bichromatic laser beams. In this section, we derive formulas for the magnitude of the interference fringes of three types of the three-level AIs.

The following first two interferometers are composed of four monochromatic laser beams, two of which have frequency ω_a and the other two have frequency ω_b . When the atom is irradiated by a sequence of $\omega_a - \omega_a - \omega_b - \omega_b$ (type A), an AI is produced by one pair of wave packets whose atomic states in the central zone are the ground state. When it is irradiated by a sequence of $\omega_a - \omega_b - \omega_a - \omega_b$ (type B), the other AI is produced by the other pair of wave packets whose atomic states in the central zone have different excited states. The last AI is composed of two bichromatic laser beams of frequencies ω_a and ω_b (type C). It corresponds to the degenerated configuration of $\omega_a - \omega_b - \omega_a - \omega_b$, whose first two and last two laser beams overlap perfectly.

A. Type A: $\omega_a - \omega_a - \omega_b - \omega_b$

The AI with a configuration of $\omega_a - \omega_a - \omega_b - \omega_b$ is shown in Fig. 2. The beam spacing D between the first and second beams is equal to that of the third and the fourth beams. The AI is composed of two trajectories. One is the atomic trajectory where the atom is excited to $|a\rangle$ after the first beam, decayed to $|g\rangle$ at the second beam, not excited at the third beam, and interacts with the fourth laser beam again. The other atomic trajectory is the one where the atom is in $|g\rangle$ throughout the first and second beams and excited to $|b\rangle$ at the third beam. Thus, the two trajectories make a closed loop at the fourth beam and interfere. This interferometer can be described using case I and case II in Sec. II. From Eq. (11), the interaction of the atom with ω_a in the matrix form is expressed by

$$e^{i(\Delta_a/2)\tau} \begin{pmatrix} A_{n,b} & 0 & 0 \\ 0 & A_{n,a} & B_n e^{-i\phi_n} \\ 0 & C_n e^{i\phi_n} & D_n \end{pmatrix}, \quad n=1,2, \quad (16)$$

where τ is the interaction time and n is the order number of the laser beams. The interaction with ω_b is

$$e^{i(\Delta_b/2)\tau} \begin{pmatrix} A_{n,b} & 0 & B_n e^{-i\phi_n} \\ 0 & A_{n,a} & 0 \\ C_n e^{i\phi_n} & 0 & D_n \end{pmatrix}, \quad n=3,4. \quad (17)$$

In Eqs. (16) and (17),

$$A_{n,l} = \exp\left\{i\left(\Delta_l - \frac{\Delta_m}{2}\right)\tau\right\},$$

$$A_{n,m} = \cos\frac{\Omega'_m}{2}\tau + i\frac{\Delta_m}{\Omega'_m}\sin\frac{\Omega'_m}{2}\tau,$$

$$B_n = C_n = i\frac{\Omega_m}{\Omega'_m}\sin\frac{\Omega'_m}{2}\tau,$$

$$D_n = \cos\frac{\Omega'_m}{2}\tau - i\frac{\Delta_m}{\Omega'_m}\sin\frac{\Omega'_m}{2}\tau, \quad (18)$$

where $m=a$ and $l=b$ for $n=1,2$, and $m=b$ and $l=a$ for $n=3,4$. The final probability amplitudes after interactions $\varphi_{Rf} = {}^t(c_b, c_a, c_g)_f$ can be given by

$$\begin{pmatrix} c_b \\ c_a \\ c_g \end{pmatrix}_f = e^{i(\Delta_a + \Delta_b)\tau} \begin{pmatrix} D_1 D_2 D_3 B_4 e^{-i\phi_4} + B_1 C_2 D_3 B_4 e^{i(\Delta_a T - \phi_1 + \phi_2 - \phi_4)} \\ + D_1 D_2 B_3 A_{4,b} e^{i(\Delta_b T - \phi_3)} + B_1 C_2 B_3 A_{4,b} e^{i\{(\Delta_a + \Delta_b)T - \phi_1 + \phi_2 - \phi_3\}} \\ D_1 B_2 A_{3,a} A_{4,a} e^{i\{\Delta_a(T+T') - \phi_2\}} + B_1 A_{2,a} A_{3,a} A_{4,a} e^{i\{\Delta_a(2T+T') - \phi_1\}} \\ D_1 D_2 D_3 D_4 + B_1 C_2 D_3 D_4 e^{i(\Delta_a T - \phi_1 + \phi_2)} + D_1 D_2 B_3 C_4 e^{i(\Delta_b T - \phi_3 + \phi_4)} \\ + B_1 C_2 B_3 C_4 e^{i\{(\Delta_a + \Delta_b)T - \phi_1 + \phi_2 - \phi_3 + \phi_4\}} \end{pmatrix}. \quad (19)$$

The signal of the interference fringes is observed as the fluorescence signals from the excited states after the interactions. The interference signal is included in the fluorescence signal when the atom decays from $|b\rangle$. However, it is difficult to distinguish the signal from the states $|a\rangle$ and $|b\rangle$. The signal is observed as the total fluorescence signal. Therefore, the interference signal is equal to the subtraction of the probability of the ground state $|g\rangle$ from unity. The time interval when the atom passes through the beam spacing D is $T = D/v_x$. The terms with an exponential function of $\Delta_a T$ and $\Delta_b T$ vanish by the integral of v_z , because the transverse velocity distribution of the atom is larger than $1/kT$. Then, the population probability of the atom in the excited states is

$$W = 1 - |D_1 D_2 D_3 D_4|^2 - |B_1 C_2 D_3 D_4|^2 - |D_1 D_2 B_3 C_4|^2 \\ - |B_1 C_2 B_3 C_4|^2 - 2|D_1 D_2 B_3 C_4 B_1^* C_2^* D_3^* D_4^*| \\ \times \cos\{(\Delta_b - \Delta_a)T - \phi_3 + \phi_4 + \phi_1 - \phi_2 + \varphi\}, \quad (20)$$

where

$$e^{i\varphi} = \frac{D_1 D_2 B_3 C_4 B_1^* C_2^* D_3^* D_4^*}{|D_1 D_2 B_3 C_4 B_1^* C_2^* D_3^* D_4^*|}. \quad (21)$$

The interference fringes result from the term which is proportional to a function of cosine in the above equation. The phase of fringes depends on three parts, which are $(\Delta_b - \Delta_a)T$, the difference of phases between laser beams, and the difference of amplitudes between laser beams denoted by Eq. (21) [18]. From the first part and Eq. (7),

$$(\Delta_b - \Delta_a)T = \left\{ \gamma(\omega_a - \omega_b) - \frac{E_b - E_a}{\hbar} \right\} T, \quad (22)$$

where $k_a \approx k_b$, $\delta_a \approx \delta_b$, and $\Gamma_a \approx \Gamma_b$ are assumed. It is found that the phase of interference does not depend on laser frequency, but depends on the frequency difference between the difference of ω_a and ω_b and resonance frequency of transition $|a\rangle$ - $|b\rangle$. Therefore, the Ramsey fringes occur as the detuning of the difference frequency, if the resonance frequency of transition $|a\rangle$ - $|b\rangle$ is less than 1 THz.

Using Eq. (18), the explicit probability of the atom in the excited states is

$$W = 1 - (2a_a^4 - 2a_a^2 + 1)(2a_b^4 - 2a_b^2 + 1) \\ - 2a_a^2 a_b^2 (1 - a_a^2)(1 - a_b^2) \cos\{(\Delta_b - \Delta_a)T \\ - \phi_3 + \phi_4 + \phi_1 - \phi_2 + \varphi\}, \quad (23)$$

where

$$a_a = \sqrt{1 - \left(\frac{\Omega_a}{\Omega'_a} \sin\frac{\Omega'_a}{2}\tau\right)^2},$$

$$a_b = \sqrt{1 - \left(\frac{\Omega_b}{\Omega'_b} \sin\frac{\Omega'_b}{2}\tau\right)^2}. \quad (24)$$

The maximum visibility of $V = (W_{max} - W_{min}) / (W_{max} + W_{min})$ is $1/6$ at $a_a^2 = a_b^2 = 1/2$. If $\Delta = 0$, the pulse area of each laser beam $\Omega\tau$ corresponds to a $\pi/2$ pulse. This numerical value can be confirmed easily by calculating the final population probabilities for each excited trajectories, as shown in Fig. 2.

B. Type B: $\omega_a - \omega_b - \omega_a - \omega_b$

Figure 3 shows the configuration of the AI with a sequence of $\omega_a - \omega_b - \omega_a - \omega_b$, where the frequencies of the second and the third laser beams in type A are interchanged. In this case, an atomic trajectory is a wave packet which is excited to $|a\rangle$ at the first beam and decayed to $|g\rangle$ at the third beam. The other atomic trajectory is in the state $|g\rangle$ before the second beam and excited to $|b\rangle$ at the second beam. The two trajectories make a closed loop at the fourth beam and

the interference occurs in the probabilities of states $|b\rangle$ and $|g\rangle$.

This AI is also described using the interactions of case I and case II in Sec. II. For $n=1,3$, the interaction is given by Eq. (16) with a matrix element of Eq. (18) at $m=a$ and $l=b$; while for $n=2,4$, the interaction is given by Eq. (17) with a matrix elements of Eq. (18) at $m=b$ and $l=a$. Subsequently, the final probability amplitudes of the states are given by

$$\begin{pmatrix} c_b \\ c_a \\ c_g \end{pmatrix}_f = e^{i(\Delta_a + \Delta_b)\tau} \begin{pmatrix} D_1 D_2 D_3 B_4 e^{-i\phi_4} + D_1 B_2 A_{3,b} A_{4,b} e^{i\{\Delta_b(T+T') - \phi_2\}} \\ + B_1 A_{2,a} C_3 B_4 e^{i\{\Delta_a(T+T') - \phi_1 + \phi_3 - \phi_4\}} \\ D_1 D_2 B_3 A_{4,a} e^{i\Delta_a T - \phi_3} + B_1 A_{2,a} A_{3,a} A_{4,a} e^{i\{\Delta_a(2T+T') - \phi_1\}} \\ D_1 D_2 D_3 D_4 + B_1 A_{2,a} C_3 D_4 e^{i\{\Delta_a(T+T') - \phi_1 + \phi_3\}} \\ + D_1 B_2 A_{3,b} C_4 e^{i\{\Delta_b(T+T') - \phi_2 + \phi_4\}} \end{pmatrix}. \quad (25)$$

Using Eqs. (18), the sum of the population probabilities on the excited states is calculated as

$$\begin{aligned} W = & 1 - a_a^4 a_b^4 - a_b^2 (1 - a_a^2)^2 - a_a^2 (1 - a_b^2)^2 \\ & - 2a_a a_b (1 - a_a^2)(1 - a_b^2) \cos\{(\Delta_b - \Delta_a)(T + T') \\ & - \phi_2 + \phi_4 + \phi_1 - \phi_3 + \varphi_\gamma\}, \end{aligned} \quad (26)$$

where

$$e^{i\varphi_\gamma} = \frac{D_1 B_2 A_{3,b} C_4 B_1^* A_{2,a}^* C_3^* D_4^*}{|D_1 B_2 A_{3,b} C_4 B_1^* A_{2,a}^* C_3^* D_4^*|}. \quad (27)$$

The phase of the interference depends on the same terms as described in the AI of $\omega_a - \omega_a - \omega_b - \omega_b$, however the period of the Ramsey fringes caused from $\Delta_a - \Delta_b$ is shorter than the latter because the trajectories are in the different excited states in the central zone.

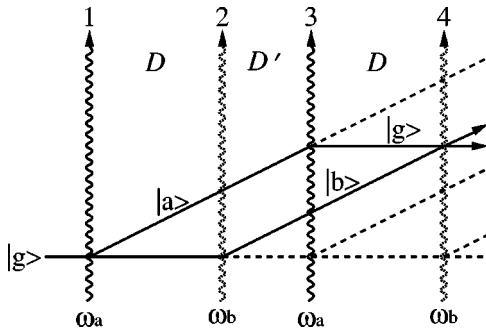


FIG. 3. AI interacting with a sequence of $\omega_a - \omega_b - \omega_a - \omega_b$, where the frequencies of the second and the third laser beams of Fig. 2 are interchanged. Details are the same as in Fig. 2.

When the excitation powers of four beams are equal, the visibility becomes a maximum at $a_a^2 = a_b^2 = (1 + \sqrt{5})/2 - \sqrt{(1 + \sqrt{5})/2} \approx 0.59$, which corresponds to the pulse area of each laser beam of about $3\pi/5$. The maximum visibility is $[-9 + 5\sqrt{5} + 2(2 + \sqrt{5})^{1/2}]/2 \approx 0.43$, which is larger than the AI of $\omega_a - \omega_a - \omega_b - \omega_b$. With four equal excitations of $\pi/2$ pulses, the visibility becomes $4/11$, which is confirmed by the calculation of the population probabilities of each excited trajectory as shown in Fig. 3. Furthermore, the visibility of 1 could be achieved if the pulse areas of the first and the fourth beams are $\pi/2$ and the second and the third are π . Therefore, this AI is one of the more attractive ones.

C. Type C: $(\omega_a, \omega_b) - (\omega_a, \omega_b)$

The three-level AI composed of two copropagating bichromatic beams of frequencies of ω_a and ω_b is shown in Fig. 4. The two trajectories are wave packets of the excited states $|a\rangle$ and $|b\rangle$ in the zone between two bichromatic laser beams. These wave packets overlap each other, if the energy difference between the states $|a\rangle$ and $|b\rangle$ is less than 1 THz. It works as a polarizing AI.

The interaction of the atom with bichromatic fields is given by Eq. (9) with a matrix element

$$\begin{pmatrix} A_{n,b} & E_n e^{i(\phi_{n,a} - \phi_{n,b})} & B_{n,b} e^{-i\phi_{n,b}} \\ F_n e^{i(\phi_{n,b} - \phi_{n,a})} & A_{n,a} & B_{n,a} e^{-i\phi_{n,a}} \\ C_{n,b} e^{i\phi_{n,b}} & C_{n,a} e^{i\phi_{n,a}} & D_n \end{pmatrix}, \quad n = 1, 2, \quad (28)$$

where E_n and F_n indicate a two-photon resonant Raman transition between states $|a\rangle$ and $|b\rangle$. In this case, the final probability amplitudes of the states are given by

$$\begin{pmatrix} c_b \\ c_a \\ c_g \end{pmatrix}_f = \begin{pmatrix} D_1 B_{2,b} e^{-i\phi_{2,b}} + B_{1,a} E_2 e^{i(\Delta_a T - \phi_{1,a} + \phi_{2,a} - \phi_{2,b})} + B_{1,b} A_{2,b} e^{i(\Delta_b T - \phi_{1,b})} \\ D_1 B_{2,a} e^{-i\phi_{2,a}} + B_{1,a} A_{2,a} e^{i(\Delta_a T - \phi_{1,a})} + B_{1,b} F_2 e^{i(\Delta_b T - \phi_{1,b} + \phi_{2,b} - \phi_{2,a})} \\ D_1 D_2 + B_{1,a} C_{2,a} e^{i(\Delta_a T - \phi_{1,a} + \phi_{2,a})} + B_{1,b} C_{2,b} e^{i(\Delta_b T - \phi_{1,b} + \phi_{2,b})} \end{pmatrix}, \quad (29)$$

and fluorescence in the end of this AI is in proportion to

$$\begin{aligned} W = & 1 - |D_1|^2 |D_2|^2 - |B_{1,a}|^2 |C_{2,a}|^2 - |B_{1,b}|^2 |C_{2,b}|^2 \\ & - 2|B_{1,b} C_{2,b} B_{1,a}^* C_{2,a}^*| \cos\{(\Delta_b - \Delta_a)T + \phi_{1,a} \\ & - \phi_{2,a} - \phi_{1,b} + \phi_{2,b} + \varphi_{bbaa}\}, \end{aligned} \quad (30)$$

where

$$e^{i\varphi_{bbaa}} = \frac{B_{1,b} C_{2,b} B_{1,a}^* C_{2,a}^*}{|B_{1,b} C_{2,b} B_{1,a}^* C_{2,a}^*|}. \quad (31)$$

The derivation of the matrix elements in Eq. (28) is generally difficult. However, in case III 1 “ $\Delta_a = \Delta_b = \Delta$ ” and case III 2 “ $\Delta_a = -\Delta_b = \Delta$ and $\Omega_a = \Omega_b = \Omega$,” in Sec. II, they could be obtained easily.

1. Case of $\Delta_a = \Delta_b = \Delta$

When the detuning of the laser frequency ω_a from the resonance transition of states $|g\rangle$ - $|a\rangle$ is the same as that of ω_b from the resonance transition of $|g\rangle$ - $|b\rangle$, using Eq. (14) matrix elements of the interaction in Eq. (28) are given as follows:

$$A_{n,m} = \frac{\Omega_m^2}{\Omega_e^2} \cos \frac{\Omega'}{2} \tau + i \frac{\Omega_m^2 \Delta}{\Omega_e^2 \Omega'} \sin \frac{\Omega'}{2} \tau + \frac{\Omega_l^2}{\Omega_e} e^{-i(\Delta/2)\tau},$$

$$B_{n,m} = C_{n,m} = i \frac{\Omega_m}{\Omega'} \sin \frac{\Omega'}{2} \tau,$$

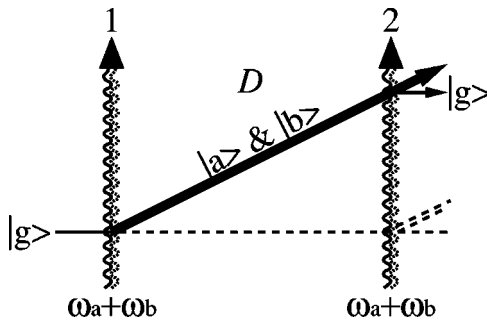


FIG. 4. AI interacting with a sequence of (ω_a, ω_b) - (ω_a, ω_b) . The atom interacts with two laser beams which are indicated by double wavy lines. The frequencies of the laser beams are ω_a and ω_b . The interference of fringes occurs due to the phase difference between the wave packets of two excited states $|a\rangle$ and $|b\rangle$ in the zone between the first and the second laser beams.

$$\begin{aligned} D_n = & \cos \frac{\Omega'}{2} \tau_n - i \frac{\Delta}{\Omega'} \sin \frac{\Omega'}{2} \tau, \\ E_n = F_n = & \frac{\Omega_a \Omega_b}{\Omega_e^2} \left(\cos \frac{\Omega'}{2} \tau - e^{-i(\Delta/2)\tau} \right) + i \frac{\Omega_a \Omega_b \Delta}{\Omega_e^2 \Omega'} \sin \frac{\Omega'}{2} \tau, \end{aligned} \quad (32)$$

where $m = a$ or b , $\Omega'^2 = \Omega_a^2 + \Omega_b^2 + \Delta^2$, and $\Omega_e^2 = \Omega_a^2 + \Omega_b^2$. The sum of the population probabilities of the excited states is deduced to

$$\begin{aligned} W = & 2 \sin^2 \frac{\Omega'}{2} \tau \left[\frac{\Omega_a^2 + \Omega_b^2}{\Omega'^2} - \frac{\Omega_a^4 + \Omega_b^4}{\Omega'^4} \sin^2 \frac{\Omega'}{2} \tau \right. \\ & \left. - \frac{\Omega_a^2 \Omega_b^2}{\Omega'^4} \sin^2 \frac{\Omega'}{2} \tau \{1 + \cos(\phi_{1,a} - \phi_{2,a} - \phi_{1,b} + \phi_{2,b})\} \right]. \end{aligned} \quad (33)$$

In this case, the phase depends on only the phase difference and the amplitude difference of the laser beams. Consequently, the Ramsey fringes are not observed on the detuning of Δ . The visibility as a function of the pulse area of one bichromatic beam $\Omega' \tau$ is shown in Fig. 5, where $p = 1 + \Omega_a^2/\Omega_b^2 + \Omega_b^2/\Omega_a^2$ and $q = \Delta^2(\Omega_a^2 + \Omega_b^2)/\Omega_a^2 \Omega_b^2$. The p indicates the difference of the two intensities of the two frequency components in the bichromatic field. When $\Omega_a = \Omega_b$, $p = 3$, otherwise $p > 3$. q is in proportion to the square of the detuning Δ . As the difference of the intensities between two components increases, a increases and the width of the pulse area in order to get high visibility becomes narrower, but the maximum visibility is constant. On the other hand, as $|\Delta|$ is increased, q increases and the maximum

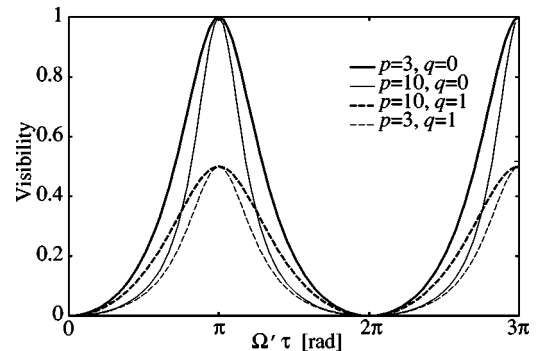


FIG. 5. Visibility of AI interacting with a sequence of (ω_a, ω_b) - (ω_a, ω_b) vs pulse area $\Omega' \tau$ in the case of $\Delta_a = \Delta_b$. $p = 1 + \Omega_a^2/\Omega_b^2 + \Omega_b^2/\Omega_a^2$ and $q = \Delta^2(\Omega_a^2 + \Omega_b^2)/\Omega_a^2 \Omega_b^2$.

visibility decreases. Thus, the velocity distribution along the laser beams, namely, Doppler shift, leads to a reduction in visibility.

2. Case of $\Delta_a = -\Delta_b = \Delta, \Omega_a = \Omega_b = \Omega$

When the three-level atoms are excited by the bichromatic fields, one of which is the detuning Δ and the Rabi frequency Ω and the other is the detuning $-\Delta$ and the same Rabi frequency Ω , the matrix element of Eq. (15) is obtained from Eq. (28):

$$\begin{aligned}
 A_{n,a} &= \frac{\Omega^2}{\Omega'^2} + \frac{\Omega^2 + 4\Delta^2}{\Omega'^2} \cos \frac{\Omega'}{2} \tau + i \frac{2\Delta}{\Omega'} \sin \frac{\Omega'}{2} \tau, \\
 A_{n,b} &= \frac{\Omega^2}{\Omega'^2} + \frac{\Omega^2 + 4\Delta^2}{\Omega'^2} \cos \frac{\Omega'}{2} \tau - i \frac{2\Delta}{\Omega'} \sin \frac{\Omega'}{2} \tau, \\
 B_{n,a} = C_{n,b} &= \frac{2\Omega\Delta}{\Omega'^2} \left(\cos \frac{\Omega'}{2} \tau - 1 \right) + i \frac{\Omega}{\Omega'} \sin \frac{\Omega'}{2} \tau, \\
 B_{n,b} = C_{n,a} &= \frac{2\Omega\Delta}{\Omega'^2} \left(1 - \cos \frac{\Omega'}{2} \tau \right) + i \frac{\Omega}{\Omega'} \sin \frac{\Omega'}{2} \tau, \\
 D_n &= \frac{4\Delta^2}{\Omega'^2} + \frac{2\Omega^2}{\Omega'^2} \cos \frac{\Omega'}{2} \tau, \\
 E_n = F_n &= \frac{\Omega^2}{\Omega'^2} \left(\cos \frac{\Omega'}{2} - 1 \right), \quad (34)
 \end{aligned}$$

where $\Omega'^2 = 4\Delta^2 + 2\Omega^2$. The sum of the population probabilities in the excited states is deduced to

$$\begin{aligned}
 W &= 1 - \frac{16}{\Omega'^8} \left(\Omega^2 \cos \frac{\Omega'}{2} \tau + 2\Delta^2 \right)^4 \\
 &\quad - \frac{8\Omega^8}{\Omega'^8} \left(\cos \frac{\Omega'}{2} \tau + 1 + 4 \frac{\Delta^2}{\Omega^2} \right)^2 \left(1 - \cos \frac{\Omega'}{2} \tau \right)^2 \\
 &\quad \times \{ 1 + \cos(-2\Delta T + \phi_{1,a} - \phi_{2,a} - \phi_{1,b} + \phi_{2,b} + \varphi_{bbaa}) \}, \quad (35)
 \end{aligned}$$

where

$$\tan \frac{\varphi_{bbaa}}{4} = \frac{\Omega' \sin \frac{\Omega'}{2} \tau}{2\Delta \left(\cos \frac{\Omega'}{2} \tau - 1 \right)}. \quad (36)$$

The Ramsey fringes with a fringe cycle of π/T appears on the detuning of Δ . The visibility versus the pulse area of each excitation $\Omega' \tau$ is shown in Fig. 6, where $q = 2\Delta^2/\Omega^2$, which is in proportion to the square of the detuning Δ . In the case of $0 \leq q \leq 1$, the pulse area for the maximum visibility shifts from π to 2π as q increases, but the maximum vis-

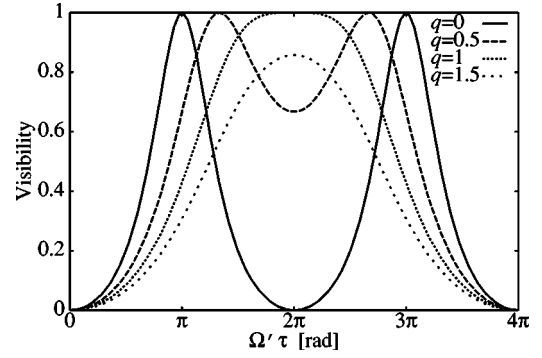


FIG. 6. Visibility of AI interacting with a sequence of $(\omega_a, \omega_b) - (\omega_a, \omega_b)$ vs pulse area $\Omega' \tau$ in the case of $\Delta_a = -\Delta_b$ and $\Omega_a = \Omega_b$. $q = 2\Delta^2/\Omega^2$.

ibility reaches to 1 at $\cos(\Omega' \tau/2) = -q$. With a further increment of q larger than 1, the maximum visibility is reduced. The visibility at $q=0$ agrees with the visibility at $p=3$ and $q=0$ in the case of $\Delta_a = \Delta_b$.

D. Comparison of the three AIs

Figure 7 shows the comparison among the visibilities of the three AIs under the condition that ω_a and ω_b are tuned to the resonance frequencies and the power of each frequency component is the same. The horizontal axis indicates the pulse area for one frequency component in the one laser beam. Therefore, the pulse area for the bichromatic fields is $\sqrt{2}$ times as large as the value of the horizontal scale. Consequently, the total power of the laser beams is the same for the three AIs.

For a small pulse area, the three visibilities are almost the same, however, with a pulse area larger than $\pi/3$, a big difference among the three visibilities appears. This difference occurs due to the extra trajectories which do not participate in the interference fringes. (They are indicated by dashed lines in Figs. 2–4.) In type C, noninterference terms in the matrix of Eq. (29) are canceled out perfectly at the pulse area of $\pi/\sqrt{2}$ and the visibility of 1 can be obtained. Contrarily, in type A the maximum visibility is only 1/6 due to the noninterference terms. However, in the case of type B, the maxi-

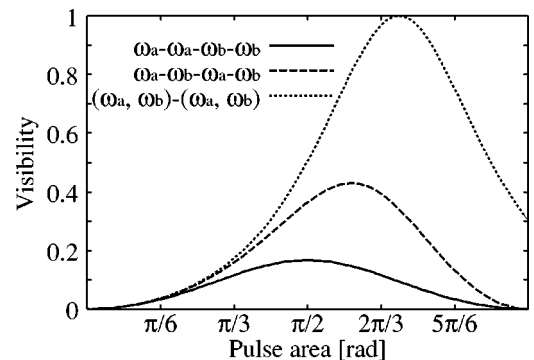


FIG. 7. Comparison of visibilities among three AIs. The horizontal axis indicates pulse area of one frequency component per laser beam.

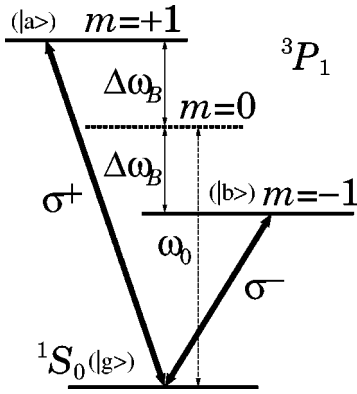


FIG. 8. Energy diagram of Ca and resonant laser frequencies under a magnetic field.

imum visibility of 1 could be obtained if the second and the third laser beams are π pulse, as we mentioned before.

IV. EXPERIMENT AND DISCUSSION

A. Experimental apparatus

As described in our previous papers [13,14], we have already actualized the three-level AIs of type A and type C, using a thermal calcium atomic beam. In the present experiment, we demonstrated the three-level AI of type B, adding to type A and C. A partial level scheme of the calcium atom is given in Fig. 8. The lifetime of the excited 3P_1 state is 0.56 ms and splits into the Zeeman substates of $m=1$, $m=0$, and $m=-1$ under the magnetic field. We use magnetic Zeeman substates of $m=1$ and $m=-1$ and the ground 1S_0 state as the three states. When the magnetic field is zero, the transition frequency of the wavelength=657 nm between the 3P_1 and 1S_0 states is denoted by ω_0 . With a magnetic-field amplitude of B , the energies of the $m=1$ and $m=-1$ states are shifted from ω_0 by $\Delta\omega_B$ and $-\Delta\omega_B$, respectively. The calcium atomic beam interacts with the two laser beams of a wavelength of 657 nm with two frequencies. One of them is a σ^+ polarized light whose frequency ω_a is near resonance to the transition between the $m=1$ and the ground states, and the other is a σ^- polarized light whose frequency ω_b is near the resonant to the transition frequency between the $m=-1$ state and the ground state.

The experimental setup of type B is shown in Fig. 9. A thermal calcium atomic beam with the most probable velocity of 780 m/s was collimated so as to produce a residual Doppler broadening of 8 MHz full width at half maximum, interacting with four laser beams at right angles, which were separated at equal spaces of $D=8.3$ mm. In the interaction zone, a homogeneous magnetic field parallel to the laser beam was applied by a Helmholtz coil. The Zeeman energy shift $\Delta\omega_B/2\pi$ was about 15 MHz. The laser beam from a high-resolution diode laser spectrometer was tuned to ω_0 and phase modulated by a resonant-type electro-optic modulator with a frequency of $\Delta\omega$. The sideband frequencies of $\omega_0 + \Delta\omega$ and $\omega_0 - \Delta\omega$ were used as ω_a and ω_b . In this situation, sweeping the carrier frequency of a laser corresponds to case III 1, while sweeping the rf frequency of the sideband corresponds to case III 2.

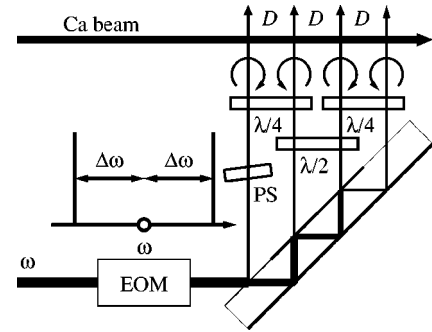


FIG. 9. Experimental setup of AI interacting with a sequence of $\omega_a - \omega_b - \omega_a - \omega_b$ (type B). The four parallel laser beams are generated by an optical plate. EOM, electro-optic modulator; PS, phase shifter; $\lambda/4$, quarter-wave plate; and $\lambda/2$, half-wave plate.

A special beam splitter was used to generate four laser beams copropagating in the same direction with equal beam spacing and equal power [13]. The diameter of each laser beam was 3 mm. Using quarter-wave plates and a half-wave plate, the first and the third laser beams were set to be a σ^+ circular polarized beam and the second and the fourth laser beams were set to be a σ^- circular polarized beam. The extinction ratio of σ^+ to σ^- was less than 0.01 and vice versa. By removing the half-wave plate, the AI of type A is constructed. A phase plate was inserted in the path of the first beam before interaction with the atomic beam. The population probability of the excited states was observed by monitoring the fluorescence from the 3P_1 state at ≈ 300 mm downstream from the interaction zones.

B. Results and discussion

The performance of type B was examined. By changing the angle of the phase plate, interference fringes appeared in the fluorescence signal. Figure 10 shows the observed interference fringes as a function of the angle of the phase plate, together with that of type A. The period of the former fringes is almost the same as that of the latter, but the size of the former is smaller than that of the latter, which seems to be inconsistent with the theoretical prediction. We will return to discuss it later.

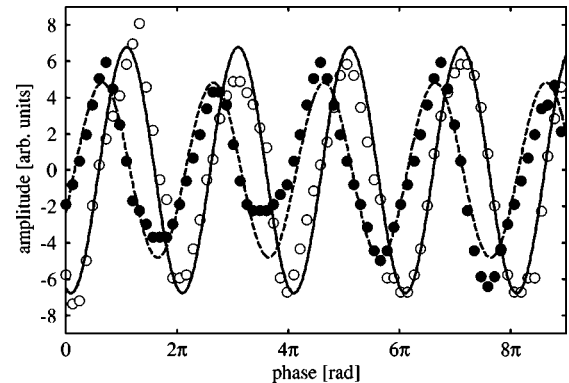


FIG. 10. Observed interference fringes of the AI as a function of the angle of the phase plate. Open circle (O); AI interacting with a sequence of $\omega_a - \omega_a - \omega_b - \omega_b$ (type A). Closed circle (●); AI interacting with a sequence of $\omega_a - \omega_b - \omega_a - \omega_b$ (type B).

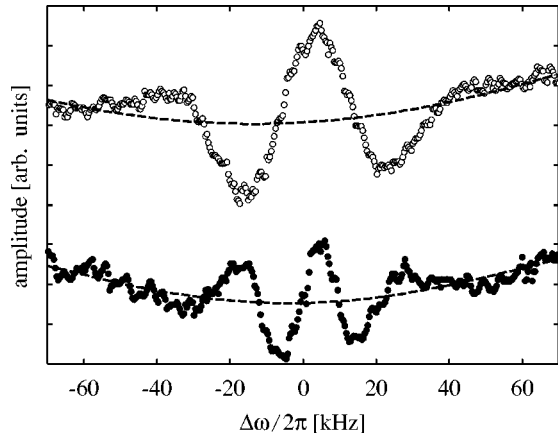


FIG. 11. Ramsey fringes observed by the tuning of $\Delta\omega$. Open circle (\circ); AI interacting with a sequence of $\omega_a - \omega_a - \omega_b - \omega_b$ (type A). Closed circle (\bullet); AI interacting with a sequence of $\omega_a - \omega_b - \omega_a - \omega_b$ (type B).

On the other hand, the Ramsey fringes of type B were observed by the tuning of $\Delta\omega$ or changing the strength of the magnetic field, as shown in Fig. 11, together with the Ramsey fringes of type A. The period of the Ramsey fringe is 43 ± 1 kHz/cycle for type B, while it is 23 ± 1 kHz/cycle for type A. This verifies Eq. (26) that the Ramsey fringes of type B depend on a reciprocal number of the spacing between the first and the third laser beams, which is twice the spacing between the first and the second laser beams.

Figure 12 shows the measured size of the Ramsey fringes for the AI of type C for various beam spacing D . The fringe size decreases as D increases according to $\exp(-D/D_0)$. The $1/e$ attenuation length D_0 is 13 ± 1 mm. There will be several reasons why it decreases, e.g., inhomogeneity of the magnetic field, scattering with background gas, or beam divergence, etc. The ratio of the fringe size at $2D$ to that at D is 0.53. For the AI of type B, the real beam spacing for the interference is $2D$. If this reduction ratio is compensated for the fringe size of type B, it becomes larger than that of type A, which is consistent with the theoretical prediction. Therefore, we could conclude that the fringe size of type B is larger than that of type A.

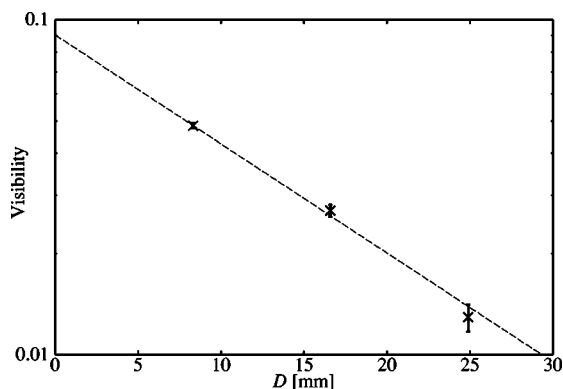


FIG. 12. Visibility of the Ramsey fringes for the AI interacting with a sequence of $(\omega_a, \omega_b) - (\omega_a, \omega_b)$ (type C) vs beam spacing D .

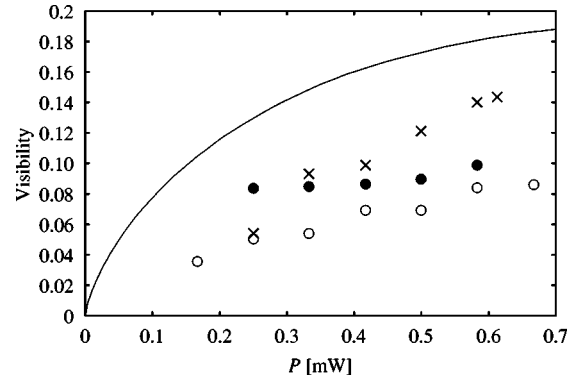


FIG. 13. Visibilities of three types of the AIs as a function of the laser power of the single transition P , with a calculated visibility for the AI excited by a sequence of $(\omega_a, \omega_b) - (\omega_a, \omega_b)$ (solid line). Open circle (\circ); AI of $\omega_a - \omega_a - \omega_b - \omega_b$ (type A). Closed circle (\bullet); AI of $\omega_a - \omega_b - \omega_a - \omega_b$ (type B). Cross (\times); AI of $(\omega_a, \omega_b) - (\omega_a, \omega_b)$ (type C).

Finally, the dependencies of the visibilities on the excitation power of each frequency component were compared for the three AIs, where the visibilities at $D=0$ mm estimated from the attenuation length are used. The laser power of 0.6 mW corresponds to the $\pi/2$ pulse area for atoms with the most probable velocity [19]. The visibility of the AI of type C is the largest of the three AIs, being 0.15 at the excitation power of 0.6 mW for each frequency component of one bichromatic beam, while that of type A is 0.09.

The shapes of the dependencies are similar to the theoretical results in Fig. 7, but the magnitudes of the visibilities are about a quarter of the theoretical ones. In order to compare the visibility with the experimental value, we must take into account the specific features of the divergent thermal calcium atomic beam. Therefore, we calculated a convolution of the probability function of Eq. (33) for the AI of type C and the beam divergence Gaussian function, and finally integrated it with the probability of the velocity having the Maxwellian velocity distribution at oven temperature [18]. The calculated visibility for type C is also shown in Fig. 13 by a curved line. The calculated results are larger than the experimental ones, but it has been found that the behavior of the experimental results is fairly well described by the calculation. The residual discrepancy may be caused by a simple assumption in the calculation and by the difficulty of achieving perfect alignment in the experiment.

V. CONCLUSION

We have derived the theoretical equation for the interaction of three-level atoms with bichromatic fields, based on the single-transition operators. The interference fringes and visibilities were calculated for three types of the three-level atom interferometers with bichromatic fields. On the other hand, we have demonstrated several types of the three-level AIs using a thermal calcium atomic beam with Zeeman sub-levels in the excited states. The experimental results were well explained by the theoretical results. It is shown that the three-level AI with two bichromatic fields has the largest visibility for the same excitation power for each frequency

component, theoretically and experimentally. The three-level AI with two laser beams of bichromatic fields was used successfully to observe the Aharonov-Casher phase directly in real time [14]. Thus, the three-level atom interferometer will become a powerful tool for investigating properties between the excited states. This three-level atom interferometer will also make it possible to construct itself in time domain using cold atoms and pulsed laser fields [20]. Then the discrepancy of the experimental visibility with the calculated one will be removed, because atoms have the same pulse area regardless of their velocity. We will attempt to use this time-domain

three-level AI to measure Berry's phase between $m = +1$ and -1 states [21].

ACKNOWLEDGMENTS

The authors would like to thank Mamoru Machiya and Kiichi Suzuki for their contribution to the experiment. They are also grateful to Takayuki Kurosu for his suggestive discussion. S. Y. and K. H. greatly appreciate the support from the Japan Society for the Promotion of Science for Young Scientists.

-
- [1] G. Wilpers, T. Binnewies, C. Degenhardt, U. Sterr, J. Helmcke, and F. Riehle, *Phys. Rev. Lett.* **89**, 230801 (2002).
- [2] T.L. Gustavson, P. Bouyer, and M.A. Kasevich, *Phys. Rev. Lett.* **78**, 2046 (1997).
- [3] A. Peters, K.Y. Chung, and S. Chu, *Nature (London)* **400**, 849 (1999).
- [4] K. Zeiske, G. Zinner, F. Riehle, and J. Helmcke, *Appl. Phys. B: Lasers Opt.* **60**, 205 (1995).
- [5] C.J. Bordé, *Phys. Lett. A* **140**, 10 (1989).
- [6] C.J. Bordé, C. Salomon, S. Avrillier, A. van Lerberghe, C. Bréant, D. Bassi, and G. Scoles, *Phys. Rev. A* **30**, 1836 (1984).
- [7] A. Morinaga and Y. Ohuchi, *Phys. Rev. A* **51**, R1746 (1995).
- [8] A. Morinaga, M. Nakamura, T. Kurosu, and N. Ito, *Phys. Rev. A* **54**, R21 (1996).
- [9] M. Kasevich and S. Chu, *Phys. Rev. Lett.* **67**, 181 (1991).
- [10] K. Moler, D.S. Weiss, M. Kasevich, and S. Chu, *Phys. Rev. A* **45**, 342 (1992).
- [11] H. Hinderthür, A. Pautz, V. Rieger, F. Ruschewitz, J.L. Peng, K. Sengstock, and W. Ertmer, *Phys. Rev. A* **56**, 2085 (1997).
- [12] M. Weitz, T. Heupel, and T.W. Hänsch, *Phys. Rev. Lett.* **77**, 2356 (1996).
- [13] S. Yanagimachi, K. Mizobuchi, and A. Morinaga, *Phys. Rev. A* **64**, 041601(R) (2001).
- [14] S. Yanagimachi, M. Kajiro, M. Machiya, and A. Morinaga, *Phys. Rev. A* **65**, 042104 (2002).
- [15] D. Suter, *The Physics of Laser-Atom Interactions* (Cambridge University Press, New York, 1997), Chap. 3.
- [16] A. Wokaun and R.R. Ernst, *J. Chem. Phys.* **67**, 1752 (1977).
- [17] S. Yanagimachi, Y. Omi, and A. Morinaga, *Phys. Rev. A* **57**, 3830 (1998).
- [18] Y. Omi and A. Morinaga, *Appl. Phys. B: Lasers Opt.* **67**, 621 (1998).
- [19] F. Riehle, A. Morinaga, J. Ishikawa, T. Kurosu, and N. Ito, *Jpn. J. Appl. Phys., Part 2* **31**, L1542 (1992).
- [20] T. Trebst, T. Binnewies, J. Helmcke, and F. Riehle, *IEEE Trans. Instrum. Meas.* **50**, 535 (2001).
- [21] M.V. Berry, *Proc. R. Soc. London, Ser. A* **392**, 45 (1984).